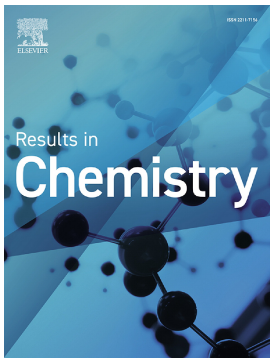

Coupled PCL hydrolysis and cellulose acetate deacetylation in cryo-coaxial core-shell fibres for wettability and TGF-β3 release control

Lauryna Bagdoniene, Aiste Pupiute, Edvardas Bagdonas, Eiva Bernotiene, Darius Ciuzas, Eidvyle Gasiulyte, Odeta Baniukaitiene, Dainius Martuzevicius, Edvinas Krugly

PII: S2211-7156(26)00300-0

DOI: https://doi.org/10.1016/j.rechem.2026.103326

Reference: RECHEM 103326

To appear in: *Results in Chemistry*

Received date: 25 February 2026

Accepted date: 17 April 2026

Please cite this article as: L. Bagdoniene, A. Pupiute, E. Bagdonas, et al., Coupled PCL hydrolysis and cellulose acetate deacetylation in cryo-coaxial core-shell fibres for wettability and TGF-β3 release control, *Results in Chemistry* (2024), https://doi.org/10.1016/j.rechem.2026.103326

Coupled PCL Hydrolysis and Cellulose Acetate Deacetylation in Cryo-Coaxial Core-Shell Fibres for Wettability and TGF-β3 Release Control

Lauryna Bagdoniene[1], Aiste Pupiute[1], Edvardas Bagdonas[2], Eiva Bernotiene[2], Darius Ciuzas[1], Eidvyle Gasiulyte[1], Odeta Baniukaitiene[1], Dainius Martuzevicius[1] and Edvinas Krugly[1*]

[1] Faculty of Chemical Technology, Kaunas University of Technology, Kaunas, Lithuania

[2] Department of Regenerative Medicine, Centre for Innovative Medicine, Vilnius, Lithuania

[*] Corresponding author. Faculty of Chemical Technology, Kaunas University of Technology, Radvilenu Rd. 19, Kaunas, Lithuania. *E-mail address:* edvinas.krugly@ktu.lt, https://orcid.org/0000-0001-5643-0614

Abstract

Porous poly(ε-caprolactone)-hydroxyapatite/cellulose acetate (PCL-HAP/CA) core-shell fibrous scaffolds were fabricated by cryo-coaxial electrospinning and post treated by controlled alkaline hydrolysis to modify their surface chemistry and wettability. This treatment induced partial hydrolysis of the PCL ester bonds and deacetylation of CA, thereby increasing the number of hydroxyl and carboxyl groups on the scaffold surface. These changes were evaluated by Fourier transform infrared spectroscopy and Toluidine Blue O assay. The scaffold morphology and core-shell structure were analysed using scanning and transmission electron microscopy, whereas the thermal, structural, and mechanical changes were assessed using thermogravimetric analysis, differential scanning calorimetry, X-ray diffraction, and tensile testing. Alkaline hydrolysis markedly improved scaffold hydrophilicity, decreasing the water contact angle from 94.7 ± 2.8° to 16.5 ± 5.1° after 25 min of treatment, and increased phosphate buffered saline uptake. The fibrous structure was preserved after shorter treatment times, whereas prolonged treatment induced local fibre damage. After loading with transforming growth factor β3, the alkaline hydrolysis treated scaffolds showed a lower day-1 burst release than the untreated scaffolds (30.7% and 39.4%, respectively) and maintained gradual release over 7 days. These results show that alkaline hydrolysis can be used as a post treatment method to increase the surface functionality and hydrophilicity of cryo-coaxially electrospun PCL-HAP/CA core-shell scaffolds and to reduce the initial burst release of TGF-β3.

Keywords: alkaline hydrolysis treatment, controlled TGF-β3 release, enhanced surface properties, fibrous scaffolds.

1. Introduction

Treating cartilage defects remains a major challenge in modern orthopedics [1,2]. Cartilage protects joints against friction and enables movement, however, the regenerative capacity of damaged articular cartilage is limited, and untreated defects eventually lead to osteoarthritis [3,4]. Metal and plastic prostheses are currently used for bone and cartilage replacement, however, friction and wear can cause implant degradation and inflammation of adjacent tissues [5,6]. Therefore, cartilage regeneration implants and scaffolds are increasingly being explored as alternative strategies [7]. Tissue implants or scaffolds composed of different materials and structures can be adapted to promote the regeneration of defective natural tissues [8]. To achieve this, the scaffold must possess biocompatibility, biodegradability, and sufficient hydrophilicity, which are important for nutrient diffusion, cell attachment, and cell migration throughout the scaffold volume [9,10]. Natural additives, such as cellulose (CEL) and hydroxyapatite (HAP), have been widely used to improve scaffold performance and bioactivity [11,12].

Electrospinning is one of the most widely used methods for the fabrication of fibrous scaffolds because it enables the production of fibres with high surface area and extracellular matrix like (ECM) morphology [13]. Recent developments show that electrospinning has advanced from conventional single fluid systems to coaxial and other multi chamber configurations, allowing better control of fibre architecture, compartmentalisation of active compounds, and release behaviour [14–16]. The morphology and internal structure of electrospun fibres are strongly influenced by the solution and process parameters, including viscosity, flow rate, applied voltage, and collection distance [17]. In addition, most electrospinning studies are performed under conventional collection conditions, whereas cryo-electrospinning enables fibre collection in the presence of ice crystals, which can increase scaffold pore size and improve the openness of the fibrous network [17,18]. Coaxial

electrospinning is particularly useful for producing layered fibres because the shell can determine the initial interaction with the surrounding medium, whereas the core can provide structural support and serve as a reservoir for active compounds [15,19]. Recent reviews and research studies on core-shell and multi chamber electrospinning confirm that these architectures can be used to regulate loading location, protect sensitive compounds, and modify release profiles [15,16]. However, fewer studies have addressed fibrous systems in which the shell layer is not only a barrier but also a chemically transformable compartment that can be converted after scaffold fabrication.

Poly(ε-caprolactone) (PCL), one of the most commonly used polymeric materials, is characterised by good processability, biodegradability, and mechanical stability, however, its low hydrophilicity and limited density of accessible functional groups restrict further biofunctionalisation and growth factor interactions [20]. Various chemical modifications have been used to increase the surface reactivity of PCL based scaffolds, including ozonation, alkaline hydrolysis, and grafting reactions [21,22]. Recent studies have further shown that surface functionalization of PCL scaffolds with peptide containing or bioactive coatings can improve wettability and cell interactions, while also emphasizing the need for controlled and well characterized modification procedures [23–25].

In this study, cryo-coaxial electrospinning was used to fabricate a fibrous scaffold with an enhanced pore size, comprising a PCL-HAP core and a cellulose acetate (CA) shell. This design was selected to combine the structural role of the PCL-HAP core with a shell layer that could be modified after fabrication. The selected alkaline hydrolysis treatment was expected to produce a dual effect by partially hydrolysing the PCL surface and simultaneously deacetylating CA to CEL, thereby increasing the concentration of hydroxyl and carboxyl groups and improving the hydrophilicity of the scaffold surface [26,27]. As transforming growth factor-beta 3 (TGF-β3) plays an important role in cartilage regeneration and

chondrogenic differentiation, it was selected as a growth factor for scaffold loading and release evaluation [28].

The effect of alkaline hydrolysis on cryo-coaxial PCL-HAP/CA core-shell scaffolds is still not well defined. Most published studies address either PCL modification or CA conversion alone, whereas the coupled effect of PCL hydrolysis and CA deacetylation within a single fibrous scaffold has received less attention. It also remains unclear how treatment time affects the surface chemistry, wettability, morphology, and growth factor release in the same system. Therefore, it was hypothesised that the controlled alkaline hydrolysis of cryo-coaxially electrospun PCL-HAP/CA core-shell scaffolds would increase the number of surface hydroxyl and carboxyl groups, improve wettability and PBS uptake, and reduce the initial TGF-β3 burst release without fully disrupting the fibrous architecture. Based on this hypothesis, the present study evaluated the effect of alkaline hydrolysis time on scaffold morphology, physicochemical properties, and *in vitro* TGF-β3 release.

2. Methods

2.1 Materials

Poly[ε]caprolactone (PCL, IUPAC name: (1,7)-Polyoxepan-2-one, CAS: 24980-41-4, Mn ~ 80 kDa, Cat. No: 440744), cellulose acetate (CA, 39.7% acetyl content, Mn~50 kDa, CAS: 9004-35-7), hydroxyapatite (HAP, <15µm particle size, CAS: 1306-06-5), Toluidine Blue O (TBO, Mw: 305.83 g/mol, CAS: 92-31-9), Dulbecco's Phosphate Buffered Saline (PBS RNBH1585), sodium dodecyl sulfate (SDS, ≥98.5%, CAS: 151-21-3), aluminum foil (Lot No. 515981) and TGF-β3 ELISA kit (Cat. No.: DY243, R&D Systems, Bio-techne Brand, USA) were purchased from Sigma-Aldrich Corp. (USA). Sodium hydroxide (NaOH, CAS N 1310-73-2) was purchased from Eurochemicals (Spa, Italy). Ethanol (96.3%, food origin) was purchased from Stumbras (Lithuania). Growth factors (Human TGF-β3 Recombinant Protein,

Cat. No: RP-8600, Invitrogen, USA) was obtained in a freeze-dried form and used without further purification.

2.2 The conceptual design of the enhanced pore size core-shell fibrous scaffolds

A fibrous scaffold with a PCL-HAP core and a CA shell was designed using cryo-coaxial electrospinning to obtain an interconnected structure with an enhanced interfibrous pore size. After fabrication, the scaffolds were treated with 0.25 M NaOH to modify the outer fibre surface. Under these conditions, partial hydrolysis of ester bonds on the PCL surface and deacetylation of CA were expected to increase the concentration of hydroxyl and carboxyl groups and to convert part of the shell layer to cellulose. After surface modification, TGF-β3 was loaded onto the scaffolds, and its *in vitro* release properties were investigated.

2.3 Fabrication of core-shell fibrous scaffolds

A core-layer polymer solution was prepared by dissolving the PCL pellets in a 2:3 (v/v) mixture of acetone and N, N-dimethylformamide and heating to 40 °C on an LBX H03D series magnetic stirrer (3 L, IBX Instruments, Spain) at 200 rpm for 6 h. HAP powder was then added to the final mixture at a concentration of 10% (w/v) PCL, and stirring was continued for 12 h to obtain a homogeneous solution. A shell layer polymer solution was prepared by dissolving CA powder in a 2:3 (v/v) mixture of acetone and dimethylformamide at a concentration of 17% (w/v), heating the mixture to 40 °C, and stirring at 200 rpm for 6 h.

The prepared solutions were used to fabricate core-shell fibrous scaffolds via cryo-solution electrospinning using a custom made solution cryo-electrospinning setup (Model SE-01C, Bious Labs, Lithuania, Fig. 1).

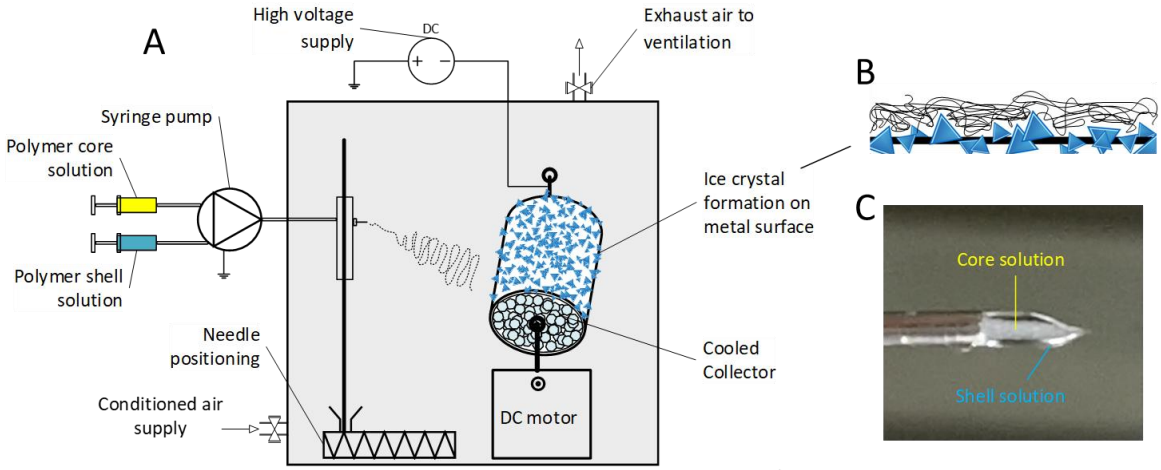

Fig. 1. Cryo-electrospinning setup (A), side view of fibre deposition during ice crystal formation on the collector surface (B), and side-view photograph of the tip of the coaxial needle (C).

The polymer solutions were loaded into 10 mL plastic Luer-lock syringes (B. Braun, Bethlehem, Pennsylvania, USA) fitted with a blunt 22/18 gauge coaxial steel needle (Ramé-Hart Instrument Co., USA). The flow rates of 2.0 mL/h (core) and 3 mL/h (shell) were controlled using two separate syringe pumps (RobotDigg XK-syringe-full, China), and the rotation speed of the grounded rotating cylindrical collector, which was cooled to -78.5 °C using dry ice, was set to 20 rpm, 10 cm from the tip. A high voltage of 16 ± 2 kV (dual-positive DC 0-50 kV) was applied. The chamber was maintained at a relative humidity of 30% and temperature of 30 °C. These conditions are appropriate for the formation of ice crystals on the collector during the cryo-electrospinning process. The formation of ice crystals from air humidity on the surface of the cylindrical collectors helps to enhance the interfibrous pore size distribution.

An infrared (IR) lamp was used to heat the solution to 40 °C to prevent polymer gelation in the syringe and the connecting tubes. After formation by electrospinning, the samples were frozen at -20 °C for 12 h and freeze-dried for 24 h to remove water ice from the samples and maintain an enhanced porous scaffold structure. The selected electrospinning conditions were used to maintain continuous jet formation and stable fibre collection in the cryo-coaxial setup.

Heating of the solution line with an IR lamp was necessary to limit the increase in viscosity and partial gelation of the polymer solutions in the syringes and connecting tubes during spinning.

2.4 Alkaline hydrolysis treatment of the fibrous scaffolds

Initially, cryo-coaxially electrospun PCL-HAP/CA core-shell scaffolds (50 × 80 × 0.7 mm) were immersed in 70% ethanol to enhance diffusion between the sample fibres [29]. Subsequently, the samples were placed in 100 mL of 0.25 M NaOH solution at 21 °C for a predetermined period, the concentration of which was chosen based on previous studies [22,29]. Following treatment, the samples were thoroughly washed with MilliQ water (to neutral pH) and dried in a vacuum chamber at 35 °C for 24 h to a constant weight.

2.5 Growth factor immobilization and release kinetics

TGF-β3 was reconstituted according to the manufacturer's instructions in 4 mM HCl and diluted with PBS before loading. Each scaffold disc (6 mm in diameter and approximately 2 mg) received 10 μL of TGF-β3 solution and was incubated for 1 h. The loaded samples were then frozen and freeze-dried for 24 h. For the release studies, each sample was immersed in 4 mL of PBS at 37 °C. At each sampling point (1, 3, and 7 days), the release medium was collected and replaced with fresh PBS. The collected samples were stored at 4 °C until ELISA. TGF-β3 concentration was determined using a human TGF-β3 ELISA kit, according to the manufacturer's protocol. Each condition was analysed using three independent samples.

The growth factor release profile was fitted to the nonlinear first-order, Higuchi, and Korsmeyer-Peppas kinetic models [30]. Fitting was performed using the OriginPro software (SimpleFit v3.10 app, Origin Lab Corporation, United States). The regression coefficient (R2) values generated by nonlinear regression were compared to determine the best-fitting model.

The best-suited data model was chosen to estimate the release rate constants (k) and exponent coefficients (n) of the release model, which describes the release mechanism [31]

The mathematical equations for the different release kinetic models were calculated as follows:

First order: $\ln(100 - y) = -kt$ (Eq. 1.)

Higuchi: $y = kt^{0.5}$ (Eq. 2.)

Korsmeyer-Peppas: $y = kt^{n}$ (Eq. 3.)

where *y* denotes the cumulative percentage of the drug released at time, *t* denotes the time, *k* denotes the rate constant, *and n* denotes the release exponent.

2.6 Physicochemical characterization

Morphology and fibre analysis. The fibrous scaffolds (surfaces morphology) were analysed using an scanning electron microscope (SEM, S-3400N, Hitachi, Germany). Cross-sections of the samples were analysed using transmission electron microscopy (TEM, Tecnai G2 F20 X-TWIN (FEI, Netherlands).

Mechanical testing. The mechanical properties were determined in the uniaxial tensile mode using a material testing machine (Zwick/Roell BDO-FB 0.5 TH, GmbH & Co., Ulm, Germany). The samples were cut into rectangular strips measuring 10 × 60 mm and tested at a constant crosshead speed of 5 mm/min.

*Fourier transform infrared (FTIR) spectra analysis***.** FTIR spectroscopy was used to evaluate the potential chemical modifications of the cryo-coaxially electrospun PCL-HAP/CA core-shell scaffolds. The spectra were recorded using an IR spectrometer (Spectrum GX FT-IR, Perkin Elmer Inc., USA). The scaffold samples were firmly pressed against a diamond crystal plate to ensure consistent sample-crystal contact. Spectra were collected in transmission mode from 4000 to 650 cm^{-1}, with five scans at a resolution of 4 cm^{-1}. Baseline

corrections and normalisation procedures were systematically applied using Spectrum (Perkin Elmer) software.

*Toluidine Blue O (TBO) assay***.** The number of carboxyl groups was determined using the TBO assay. The sample was incubated for 24 h at 37 °C in 3 mL of a 0.1% TBO solution prepared by dissolving it in 1mM NaOH. Unbound TBO was removed by washing the sample with NaOH. The attached TBO dye was then removed by soaking the sample in a 3 mL solution of 20% sodium dodecyl sulfate (SDS) for 24 h. The absorbance was measured at 625 nm, and the number of carboxylic groups was calculated from the calibration curve of the standard TBO solution.

Water contact angle (WCA) measurements. The WCA (θ) was measured using a Theta Lite TL 101 optical tensiometer at room temperature (20 ± 1 °C) (manufactured by Biolin Scientific and operated with OneAttension v1.0, Finland) to evaluate the hydrophilicity of the samples.

PBS uptake. PBS uptake was measured by immersing the sample discs (6 mm diameter) in PBS (pH 7.4) at 37 °C. The samples were weighed before and after immersion in 5 mL of PBS, wiped with filter paper, and PBS uptake was calculated using the following equation:

$$\text{PBS uptake } (\%) = \frac{W_w - W_d}{W_d} \cdot 100 \qquad \text{(Eq. 4.)}$$

where W_w and W_d are the weights of the wet and dry samples, respectively.

X-ray diffraction (XRD). The degree of crystallinity (CI, %) of the samples was determined by XRD analysis using a diffractometer (D8 Advance, Bruker AXS, Germany). The parameters used were Ni-filtered Cu Kα radiation, detector moving rate of 0.02°, measurement intensity of 0.5 s, 40 kV anode voltage, and 40 mA current. The CI was determined using the following equation:

$$\text{CI} = \frac{A_1}{A_2} \times 100 \qquad \text{(Eq. 5.)}$$

where A_1 is the area of the crystalline peak and A_2 is the area of all the peaks, measured using OriginPro software.

Thermogravimetric Analysis (TGA) and Differential Scanning Calorimetry (DSC). The thermal properties were evaluated using TGA and DSC. For the TGA thermal analyser (TGA 4000, Perkin Elmer, JAV), a scan was performed in a nitrogen atmosphere from 40 °C to 600 °C at 10°C/min. DSC (DSC 8500, Perkin Elmer, JAV) was conducted in a nitrogen atmosphere using an aluminum crucible and heated from 0 °C to 250 °C at a rate of 5 °C/min.

2.7 Data analysis and quality control

The geometric parameters of the fibre and pore size were measured from the SEM micrographs using image analysis software (ImageJ, University of Wisconsin-Madison, USA). The SEM image was divided into four equal quartiles, and the size distributions were estimated by measuring all the fibres in a quarter of an image, with at least 100 fibres from each image. Randomly selected pores were analysed along both the long and short pore axes. Data are expressed as the mean ± standard deviation or mean value and interquartile range (IQR), depending on the normality of the distribution results. Differences between samples were assessed using two-sample t-tests (v2021, Origin Lab Corporation, United States), with statistical significance set at $p < 0.05$. Each sample was prepared and analysed using a minimum of three specimens.

3. Results and Discussion

3.1 Effects of alkaline hydrolysis treatment on morphology of fibrous scaffolds

Randomly oriented core-shell fibrous scaffolds were produced via cryo-coaxial electrospinning. The fibre diameter of the produced fibrous scaffold is presented as median values and interquartile ranges (IQR: 25th and 75th percentiles). The median fibre diameter of the untreated fibrous scaffold was 0.6 (IQR 0.5-0.9) μm. The surface treatment of alkaline

hydrolysis influenced the fibre diameter of the fibrous scaffolds, increasing it from 0.7 (IQR 0.5-0.9) µm (1 min) to 0.9 (IQR 0.6-1.2) µm (25 min) (**Fig. 3B**). Statistical analysis showed that there was no significant difference between 1 min (0.7 (IQR 0.5-0.9) µm) and the duration of treatment of 5 min compared to the 0.6 (IQR 0.5-0.9) µm of untreated scaffolds (0 min). However, a difference in fibre diameter was observed after 25 min of alkaline hydrolysis treatment compared to that at 0 min. SEM images revealed uneven fractures in the fibrous scaffolds with the longest alkaline hydrolysis treatment duration (**Fig. 2A**). Even after 5 min, some fractures were observed, although no differences were indicated by fibre diameter analysis.

The pore size distribution was also analysed as a function of the alkaline hydrolysis treatment time. The alkaline hydrolysis of the scaffolds changed the interfibrous pore sizes, decreasing from 7.5 (IQR 5.4-9.7) µm (0 min, untreated) to 4.5 (IQR 3.5-5.5) µm (25 min of alkaline hydrolysis treatment), with all results statistically different from each other except between 5 min (5.4 (IQR 4.0-6.9) µm) and 25 min (**Fig. 3C**).

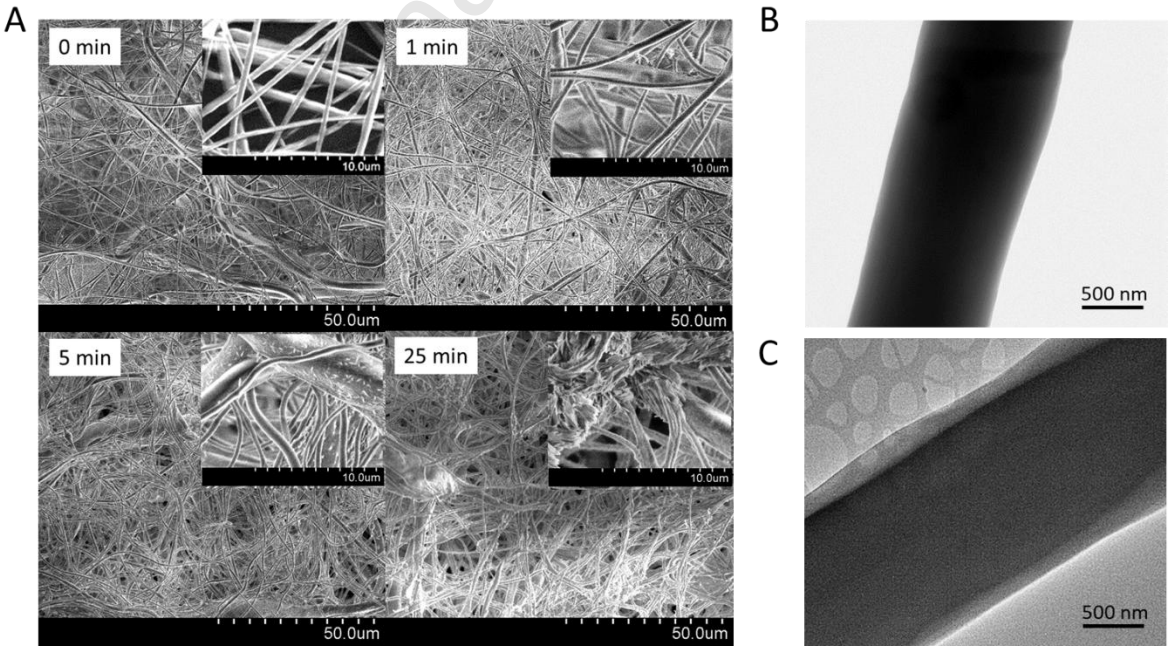

Fig. 2. Morphology of PCL-HAP/CA core-shell fibrous scaffolds fabricated by cryo-coaxial electrospinning: SEM images of alkaline hydrolysis-treated fibrous scaffolds (0, 1, 5, and 25 min) (A), TEM images of PCL (B), and PCL/CA core-shell fibres (C).

The changes in fibre diameter and pore size between the fibres of the scaffolds can be attributed to the effects of the alkaline hydrolysis treatment. During alkaline hydrolysis, the ester bonds in the polymer chains are cleaved, leading to the partial degradation of the polymer matrix [32]. This degradation causes the fibres to swell, increasing their diameter. Additionally, the deacetylation of CA to cellulose introduces hydroxyl groups, which enhance the hydrophilicity of the fibres, further contributing to the swelling effect [33]. The increased fibre diameter, combined with the partial dissolution and reorganisation of the polymer chains, resulted in a denser fibre network. This denser network reduces the size of the interfibrous pores because swollen fibres occupy more space within the scaffold structure. These morphological changes are influenced by the duration and concentration of the alkaline treatment, with longer exposure times leading to more pronounced effects on fibre swelling and pore size reduction.

The differences between the single PCL fibres **(Fig. 2B**), and PCL core-shell fibres (**Fig. 2C**) is shown in the TEM images. The shell layer (CA) was approximately five times smaller than the core diameter (1.2 μm), indicating a core-shell size ratio of 5:1, which is consistent with PCL and HAP.

3.2 Effects of alkaline hydrolysis treatment on mechanical properties of fibrous scaffolds

The mechanical properties were analysed by examining the Young's modulus and elongation as a function of the duration of the alkaline hydrolysis treatment. The results showed that the Young's modulus gradually decreased from 6.5 ± 0.8 MPa (0 min, untreated) to 3.9 ± 0.6 MPa (25 min) as the alkaline treatment time increased (**Fig. 3A**). Statistical

analysis revealed that all the results were statistically different from those of the untreated sample; however, the difference between the adjacent values was between 0 and 5 min. Furthermore, the elongation results were found to be inversely proportional to the duration of the alkaline treatment, increasing from 17.3 ± 5.8% (0 min, untreated) to 36.8 ± 5.8% (25 min).

The only statistically significant difference between the values was observed between the 0 and 25 min treatment groups. These results suggest that as the treatment duration increased, the samples became mechanically weaker but more elastic, as evidenced by the increase in relative elongation. This coherence between Young's modulus and elongation has been described in other studies [34,35]. This is because surface modification by alkaline hydrolysis treatment of the fibres causes disintegration of the crystals within the polymer chains, resulting in a more amorphous and flexible structure [36].

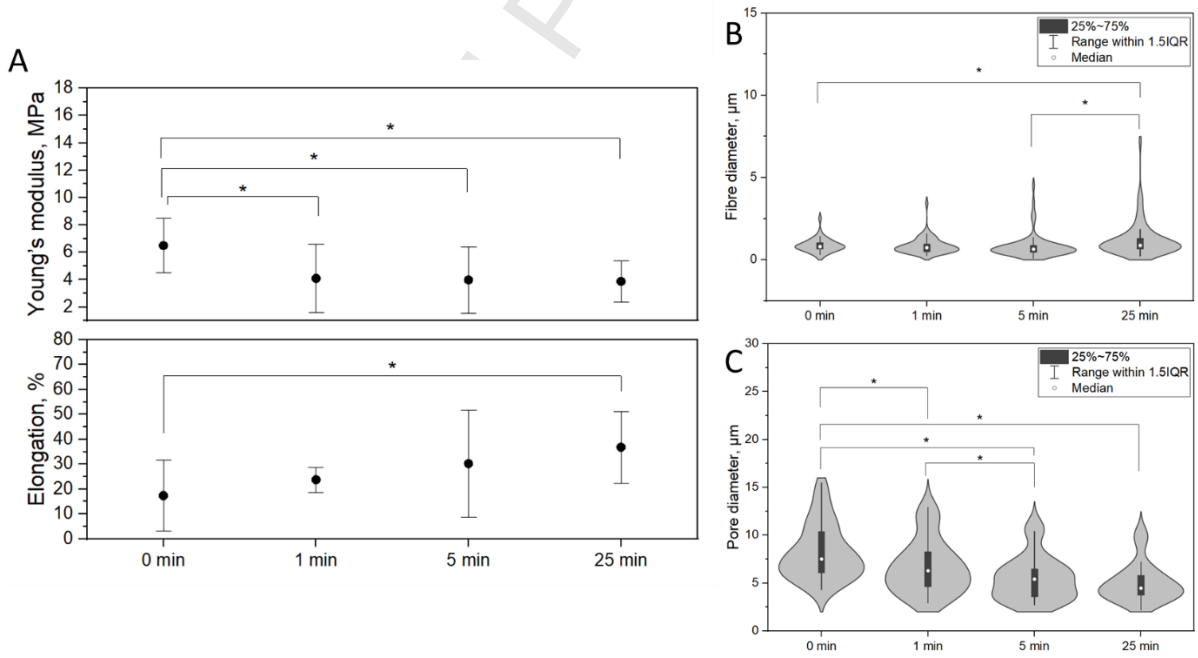

Fig. 3. Mechanical and morphological properties: Young's modulus and elongation of alkaline hydrolysis-treated PCL-HAP/CA core-shell fibrous scaffolds (0, 1, 5, and 25 min) (A), fibre diameter distributions (n=100) (B), pore diameter distributions (n=30) (C), (*) indicates statistically significant difference, $p < 0.05$.

3.3 Effects of alkaline hydrolysis treatment on chemical and physical properties of fibrous scaffolds

Chemical characterisation was conducted using FTIR and TBO assays to identify any changes after the alkaline treatment of the scaffolds (**Fig. 4 A, B**). As the samples comprised several materials, the spectra revealed the typical FTIR peaks of these materials (**Fig. 4A**).

The PCL absorption peaks at 2938 and 2868 cm^{-1} were attributed to the asymmetric and symmetric stretching of the methylene groups. Moreover, a major absorption band at 1721 cm^{-1} was associated with the carbonyl peak of the ester. Additionally, the bands at 1287, 1237, 1162, and 1035 cm^{-1} were attributed to C-O and C-C, asymmetric C-O-C, symmetric C-O-C, C-O, and C-H stretching vibrations, respectively.

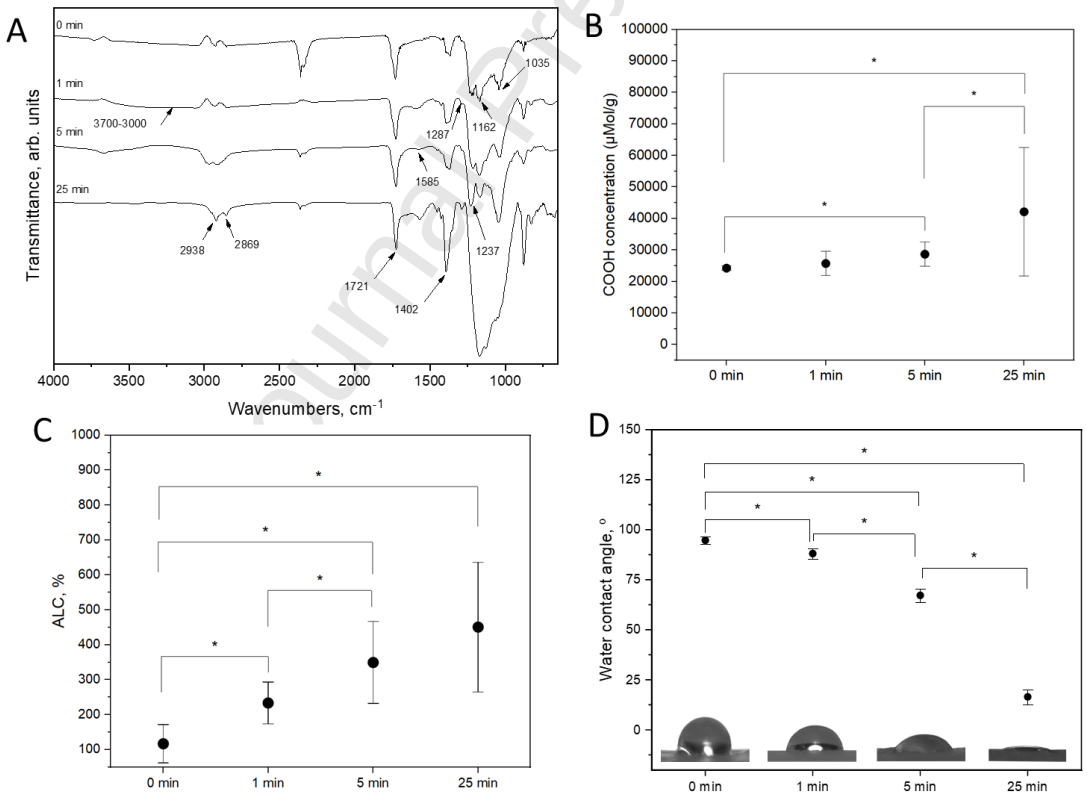

Fig. 4. FTIR spectra (A), COOH group concentration (TBO analysis) (B), PBS uptake (C) and WCA (D) of alkaline hydrolysis treated PCL-HAP/CA core-shell fibrous scaffolds, (*) indicates statistically significant difference, $p < 0.05$.

Furthermore, CA adsorption peaks at 1237 cm^{-1}, attributed to C-O-C, were observed [37]. Additionally, peaks were observed at 1585 cm^{-1} for the asymmetric group and 1402 cm^{-1} for the symmetric -COO- group [38]. Prolonged treatment led to a broad range of values from 1184 to 1040 cm^{-1}, which may be related to the conversion of CA to CEL after treatment. Similar results have been reported previously [39]. The 3700-3000 cm^{-1} broad band is related to the -OH peaks [40]. HAP particles were also present in the samples, and a typical peak was observed in the 1100-1000 cm^{-1} spectrum of the PO_4 group [41].

The complexity of the substances and the chemical interactions between the core and shell cause several characteristic band peak shifts and overlapping spectra, making it difficult to identify more HAP peaks. However, treatment with an alkaline solution increased the number of hydroxyl and carboxyl groups, resulting in a significant increase in the intensity of the peaks at 1585, 1402, and 3700-3000 cm^{-1} in the spectrum.

TBO analysis was used to validate the FTIR results by quantifying the concentration of carboxylic groups (-COOH) in the samples. As -COOH functional groups are the main components of the attachment sites of growth factors, it is essential to accurately measure their contents. The results obtained indicated that the -COOH concentration increased from $(2.4 \pm 0.03) \times 10^4$ to $(4.2 \pm 0.8) \times 10^4$ μmol/g with increasing duration of treatment from 0 to 25 min (**Fig. 4B**). There were no significant discrepancies between 0 and 1 min ($(2.6 \pm 0.2) \times 10^4$ μmol/g) and between 1 and 5 min ($(2.9 \pm 0.2) \times 10^4$ μmol/g). However, a significant difference was observed between 5 and 25 min treatments. When comparing the treated and untreated samples, a significant difference was observed when the alkaline treatment time was 5 min or longer. These results corroborate the trend observed in the FTIR analysis, which showed that the concentration of -COOH groups also increased with increasing alkaline hydrolysis duration.

WCA and PBS uptake were analysed to observe the hydrophilicity and sorption properties essential for cell growth (**Fig. 4C, D**). As the treatment duration increases, the theory suggests that the hydrophilicity of the sample also increases owing to the presence of hydrophilic functional groups (hydroxyl and carboxyl). Polar functional groups (carboxyl and hydroxyl) have a high affinity for water through polar interactions and can assemble on hydrophilic surfaces [42]. The WCA of the untreated scaffold samples was 94.7 ± 2.8°. By increasing the duration of the surface treatment via alkaline hydrolysis, the WCA changed to 88.1 ± 3.6° (1 min), 67.2 ± 4.6° (5 min), and 16.5 ± 5.1° (25 min), respectively (**Fig. 4D**). All values were statistically different from each other and were compared with those of untreated samples.

The WCA and PBS uptake results followed the same direction as the TBO data. With longer alkaline treatment, the PCL-HAP/CA core-shell scaffold surface became more hydrophilic, as reflected by the decrease in the WCA and increase in PBS uptake. The parallel changes in WCA, PBS uptake, and carboxyl group concentration indicate that alkaline hydrolysis altered the surface chemistry and water-scaffold interactions of the fibrous scaffolds. These changes may also influence the loading and release behaviours of TGF-β3. However, because the growth factor binding efficiency was not measured directly in the present study, this relationship should be interpreted as an indirect association rather than direct proof of enhanced growth factor absorption. Samples with higher PBS uptake have a greater potential to absorb growth factors and improve 3D cell spreading [43].

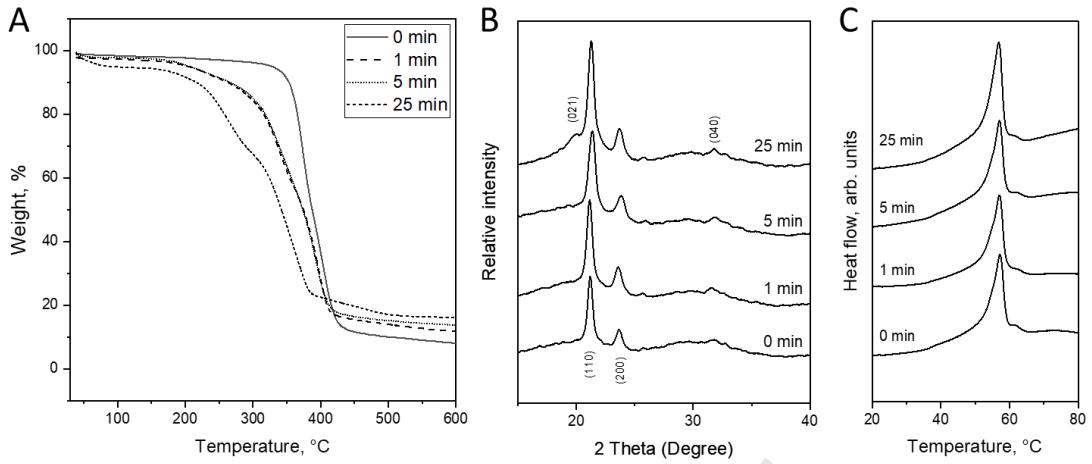

Fig. 5. *Thermogravimetric analysis (TGA) curves (A), X-ray diffractograms (XRD) (B), and differential scanning calorimetry (DSC) (C) ofthe PCL-HAP/CA core-shell fibrous scaffolds.*

The thermal properties and crystallinity of the treated samples are shown in **Fig. 5** and were analysed using TGA (**Fig. 5A**) and DSC (**Fig. 5C**). The main change in the sample weight during the heating process was observed in the temperature range of 200-500 °C. The TGA curves demonstrate similar degradation behaviours for all samples, but at different temperature ranges. The degradation temperature ranged from 347 to 429 °C for the untreated sample and from 207 to 385 °C for the sample treated for 25 min. The results for 1 and 5 min durations were similar to each other but different from those of the untreated and treated samples (25 min). Treatment durations of 0, 1, and 5 min resulted in a one-step thermal transition, which was associated with the structural decomposition of the polymer blends [44]. The 25 min treated sample showed a two-step transition, which was due to the loss related to moisture evaporation and depolymerisation of cellulose [45]. These findings confirm that alkaline treatment changes not only the functional groups on the surface of the sample fibres but also the composition of the sample by regenerating cellulose from cellulose acetate.

The decomposition temperatures of the untreated samples were higher than those of the untreated samples. However, as the treatment duration increased, the decomposition temperature decreased. This was further supported by the DSC analysis, which showed that

the melting peak decreased from 57.2 °C (0 min) to 57.1 °C (1 min) and further decreased to 57.0 °C (5 min) and 56.8 °C (25 min) during treatment.

The XRD patterns of the core-shell samples are shown in **Fig. 5B**, with the two most prominent peaks at 21°and 23.6°, which are attributed to the (110) and (200) crystallographic peaks characteristic of pure PCL polymer [46]. Additionally, the peak at (110) was assigned to the characteristic peak (002), and the wide range with a small peak at 31.6° was assigned to the crystallographic peak (040) [47]. As the treatment time increased, the CEL peak at 19° also increased, which is similar to that observed in composites where the amount of CEL increased, as CEL can act as a nucleating agent and promote PCL crystallization [48].

The crystallinity index (CI) was determined from the area of the peaks in the XRD patterns. As the treatment duration increased, the CI increased from 34.8% (0 min) to 36.1% (1 min), 37.0% (5 min), and 43.2% (25 min). This was further supported by the TGA analysis, which showed that the thermal decomposition of the samples with a longer treatment duration (25 min) included a stage of regenerated cellulose decomposition.

3.4 Effects of alkaline hydrolysis treatment on TGF-β3 release from core-shell fibrous scaffolds

TGF-β3 is one of the key growth factors involved in cell differentiation and ECM formation [49]. Therefore, incorporation of TGF-β3 into polymer scaffolds may be useful for tissue regeneration and in vitro modeling. In cartilage tissue engineering, the scaffold does not only provide structural support, but may also act as a carrier for controlled delivery of biologically active molecules. Therefore, the release profile of TGF-β3 is important, because uncontrolled release may reduce local effectiveness and shorten the period of action [28]. The release profile of TGF-β3 from the core-shell fibrous scaffolds showed an early release phase within the first day, followed by a slower release up to day 7 (**Fig. 6**).

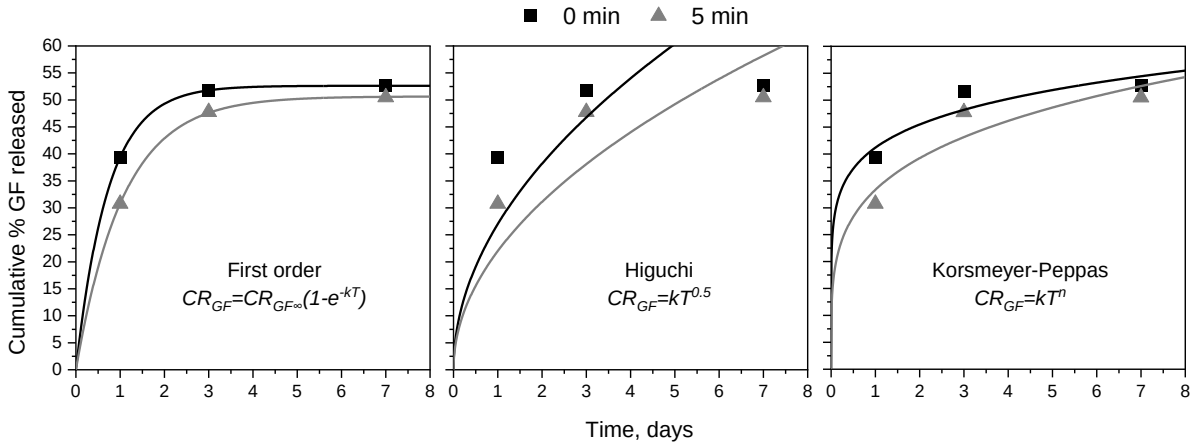

Fig. 6. Comparative fitting of TGF-β3 release data from untreated and 5 min alkaline hydrolysis-treated core-shell fibrous scaffolds.

The untreated scaffold released 39.4% of the loaded TGF-β3 within the first day, whereas the core-shell fibrous scaffolds treated with alkaline hydrolysis for 5 min released 30.7%. After 7 days, the cumulative release reached 52.7% for the untreated scaffold and 50.5% for the treated scaffold (**Table 1**). Thus, alkaline hydrolysis reduced the day-1 burst release by 8.7 percentage points while maintaining a gradual release during the remaining period.

Table 1. Comparative fitting parameters of TGF-β3 release data from untreated and 5 min alkaline hydrolysis-treated fibrous scaffolds.

Scaffold	Total Release after 7 days, %	Kinetic model						
		First order		Higuchi		Korsmeyer-Peppas		
		R^2	k	R^2	k	R^2	k	n
0 min	52.7 ± 2.63	0.99	1.38 ± 0.01	0.33	27 ± 0.1	0.66	41.2 ± 3.91	0.14 ± 0.07
5 min	50.5 ± 2.02	0.99	0.94 ± 0.01	0.33	22 ± 0.4	0.72	33.3 ± 5.08	0.23 ± 0.10

The reduced initial release from the treated scaffold may be related to the physicochemical changes induced by the alkaline hydrolysis. The treated samples showed higher hydrophilicity, higher PBS uptake, and a greater number of surface carboxyl groups, whereas the morphology analysis indicated a denser fibrous network with reduced interfibrous pore size after treatment. Together, these changes suggest that alkaline hydrolysis altered both the interaction of TGF-β3 with the fibre surface and the penetration of the

aqueous medium into the scaffold. Under these conditions, the early release phase was likely influenced by diffusion of weakly bound or surface associated TGF-β3, whereas the later phase may have been governed by slower transport through the hydrated fibrous structure. The release data were fitted to the first-order, Higuchi, and Korsmeyer-Peppas models (Table 1). Among the tested models, the first order equation showed the highest R2 values for both scaffold groups. However, because the present study included only three sampling time points, the model fitting should be interpreted as a comparative description of the release profiles rather than as definitive evidence of the release mechanism. Therefore, the lower fitted k value of the alkaline hydrolysis treated scaffold indicates a tendency towards slower release, but it does not allow a firm conclusion that the release followed first-order kinetics under all conditions. Similar observations have been reported for other scaffold systems used for TGF-β3 delivery in the literature. Surface modified PCL fibre mats released TGF-β3 in amounts that depended on the loading approach and were sufficient to induce chondrogenic differentiation of mesenchymal stromal cells [50]. PCL fibre scaffolds with chitosan-based coatings have also been used to control the spatial and temporal release of TGF-β3 and BMP-2 [51]. In another study, nanoparticle mediated delivery from microribbon based hydrogels enabled tunable TGF-β3 release and supported cartilage formation in vivo [52]. ECM derived scaffolds have also shown controlled release of most of the loaded TGF-β3 during the first 10 days of culture [53]. These studies indicate that the release behaviour depends on both the scaffold structure and the interaction between TGF-β3 and the carrier phase.

The present results show that alkaline hydrolysis can be used as a post treatment step to reduce the initial burst release of TGF-β3 from cryo-coaxially electrospun PCL-HAP/CA fibrous scaffolds. Simultaneously, the release remained gradual over 7 days. This effect is favourable for further development of cartilage regeneration and in vitro modeling scaffolds

because it may help reduce early growth factor loss while maintaining its availability during the initial stage of tissue response.

Conclusions

Cryo-coaxial electrospinning produced PCL-HAP/CA core-shell fibrous scaffolds with an enhanced interfibrous pore size. Controlled alkaline hydrolysis changed both the surface chemistry and the physical properties of the scaffolds. The treatment increased the concentration of carboxyl groups, reduced the water contact angle, increased PBS uptake, and altered the thermal and structural behaviour of the samples, which was consistent with partial PCL hydrolysis and cellulose acetate deacetylation reactions. Shorter treatment preserved the general fibrous architecture, whereas prolonged treatment induced local fibre damage. For TGF-β3 loaded scaffolds, 5 min of alkaline treatment reduced the day-1 burst release from 39.4% to 30.7% and maintained the release over 7 days. These findings show that alkaline hydrolysis can be used as a post treatment step to modify the surface properties and early release behaviour of cryo-coaxially electrospun PCL-HAP/CA scaffolds. The present release data support a comparative assessment of burst release reduction, whereas a denser sampling schedule will be required in future studies to define the release mechanism more precisely and evaluate biological performance.

Funding

This study was funded by the Research Council of Lithuania “New Generation *In Vitro* Model of Osteochondral Tissue: Synergistic Engineering of Multilayered 3D Polymer Scaffolds and Smart Hydrogels” (Grant No. S-MIP-24-38).

Conflicts of interest

The authors declare that they have no known competing financial interests or personal relationships that could influence the work reported in this study.

Data and materials availability

The data supporting the findings of this study are available from the corresponding author upon reasonable requests.

AI Disclaimer

The grammar consistency of the text of this article was improved using Paperpal by Editage (v. 42.2.6).

References

[1] M. Moradi, F. Parvizpour, Z. Arabpour, N. Zargarzadeh, M. Nazari, H. Rashnavadi, F. Sefat, S. Dehghani, M. Latifi, A. Jafarian, Articular Cartilage Injury; Current Status and Future Direction, Curr. Stem Cell Res. Ther. 19 (2024) 653–661. https://doi.org/10.2174/1574888X18666230418121122.

[2] M.T. Nguyen, S. Gronthos, Y. Zhao, V. Chandrakanthan, V.K. Truong, K. Vasilev, Overcoming challenges in cartilage regeneration: The role of chondrogenic inducers, Bioeng. Transl. Med. 11 (2025) e70079. https://doi.org/10.1002/BTM2.70079;WGROUP:STRING:PUBLICATION.

[3] M.P.F. Janssen, E.G.M. van der Linden, T.A.E.J. Boymans, T.J.M. Welting, L.W. van Rhijn, S.K. Bulstra, P.J. Emans, Twenty-Two-Year Outcome of Cartilage Repair Surgery by Perichondrium Transplantation, Cartilage 13 (2021) 860S-867S. https://doi.org/10.1177/1947603520958146.

[4] A.L. Lara-Bertrand, L. Lizarazo-Fonseca, L. Correa-Araujo, G. Salguero, I. Silva-Cote, Innovative Technologies for Articular Cartilage Repair: Research, Development, and Clinical Translation—A Narrative Review, J. Funct. Biomater. 17 (2026). https://doi.org/10.3390/JFB17030128.

[5] A. Pemmari, T. Leppänen, T. Moilanen, E. Moilanen, Gene expression in adverse reaction to metal debris around metal-on-metal arthroplasty: an RNA-seq-based study, Osteoarthritis Cartilage 26 (2018) S130. https://doi.org/10.1016/j.joca.2018.02.282.

[6] C.C. Ude, C.J. Esdaille, K.S. Ogueri, H.-M. Kan, S.J. Laurencin, L.S. Nair, C.T. Laurencin, The Mechanism of Metallosis After Total Hip Arthroplasty, Regen. Eng. Transl. Med. 7 (2021) 247–261. https://doi.org/10.1007/s40883-021-00222-1.

[7] K. Perera, R. Ivone, E. Natekin, C.A. Wilga, J. Shen, J.U. Menon, 3D bioprinted implants for cartilage repair in intervertebral discs and knee menisci, Front. Bioeng. Biotechnol. 9 (2021) 754113. https://doi.org/10.3389/fbioe.2021.754113.

[8] D. Goyal, Recent advances and future trends in articular cartilage repair, Journal of Arthroscopic Surgery and Sports Medicine 1 (2020) 159–173. https://doi.org/10.25259/JASSM_11_2020.

[9] Z. Wang, H. Le, Y. Wang, H. Liu, Z. Li, X. Yang, C. Wang, J. Ding, X. Chen, Instructive cartilage regeneration modalities with advanced therapeutic implantations under abnormal conditions, Bioact. Mater. 11 (2022) 317–338. https://doi.org/10.1016/j.bioactmat.2021.10.002.

[10] X. Yu, Y. Hu, L. Zou, S. Yan, H. Zhu, K. Zhang, W. Liu, D. He, J. Yin, A bilayered scaffold with segregated hydrophilicity-hydrophobicity enables reconstruction of goat hierarchical temporomandibular joint condyle cartilage, Acta Biomater. 121 (2021) 288–302. https://doi.org/10.1016/j.actbio.2020.11.031.

[11] M.L. Chinta, A. Velidandi, N.P.P. Pabbathi, S. Dahariya, S.R. Parcha, Assessment of properties, applications and limitations of scaffolds based on cellulose and its derivatives for cartilage tissue engineering: A review, Int. J. Biol. Macromol. 175 (2021) 495–515. https://doi.org/10.1016/j.ijbiomac.2021.01.196.

[12] Z.-X. Zhou, Y.-R. Chen, J.-Y. Zhang, D. Jiang, F.-Z. Yuan, Z.-M. Mao, F. Yang, W.-B. Jiang, X. Wang, J.-K. Yu, Facile Strategy on Hydrophilic Modification of Poly(ε-caprolactone) Scaffolds for Assisting Tissue-Engineered Meniscus Constructs In Vitro, Front. Pharmacol. 11 (2020) 471. https://doi.org/10.3389/fphar.2020.00471.

[13] Z. Mohammadalizadeh, E. Bahremandi-Toloue, S. Karbasi, Recent advances in modification strategies of pre- and post-electrospinning of nanofiber scaffolds in tissue engineering, React. Funct. Polym. 172 (2022) 105202. https://doi.org/10.1016/j.reactfunctpolym.2022.105202.

[14] S. Lian, D. Lamprou, M. Zhao, Electrospinning technologies for the delivery of Biopharmaceuticals: Current status and future trends, Int. J. Pharm. 651 (2024) 123641. https://doi.org/10.1016/J.IJPHARM.2023.123641.

[15] Y. Liu, X. Chen, X. Lin, J. Yan, D.G. Yu, P. Liu, H. Yang, Electrospun multi-chamber core-shell nanofibers and their controlled release behaviors: A review, Wiley Interdiscip. Rev. Nanomed. Nanobiotechnol. 16 (2024). https://doi.org/10.1002/WNAN.1954.

[16] B. Akhila, V. Abhijith, M. Sreedharan, L. Ravindran, A. Sathian, S. Thomas, S.M. Sadasivan, Innovations in Core–Shell Electrospinning: A Comprehensive Review in Recent Advances of Core–Shell Electrospun Polylactic Acid Nanocomposite Fibers for Potential Biomedical Applications, ACS Biomater. Sci. Eng. 11 (2025) 3826–3857. https://doi.org/10.1021/ACSBIOMATERIALS.5C00194.

[17] H. Zhou, Z. Shi, X. Wan, H. Fang, D.-G. Yu, X. Chen, P. Liu, The relationships between process parameters and polymeric nanofibers fabricated using a modified coaxial electrospinning, Nanomaterials (Basel) 9 (2019) 843. https://doi.org/10.3390/nano9060843.

[18] N. Munir, A. McDonald, A. Callanan, A combinatorial approach: Cryo-printing and electrospinning hybrid scaffolds for cartilage tissue engineering, Bioprinting 16 (2019) e00056. https://doi.org/10.1016/j.bprint.2019.e00056.

[19] D. Han, A.J. Steckl, Cover Feature: Coaxial Electrospinning Formation of Complex Polymer Fibers and their Applications (ChemPlusChem 10/2019), ChemPlusChem (Weinheim, Germany) 84 (2019) 1451. https://doi.org/10.1002/cplu.201900434.

[20] E. Malikmammadov, T.E. Tanir, A. Kiziltay, V. Hasirci, N. Hasirci, PCL and PCL-based materials in biomedical applications, J. Biomater. Sci. Polym. Ed. 29 (2018) 863–893. https://doi.org/10.1080/09205063.2017.1394711.

[21] L. Dabasinskaite, E. Krugly, O. Baniukaitiene, D. Martuzevicius, D. Ciuzas, L. Jankauskaite, L. Aukstikalne, A. Usas, The Effect of Ozone Treatment on the Physicochemical Properties

and Biocompatibility of Electrospun Poly(ε)caprolactone Scaffolds, Pharmaceutics 13 (2021) 1288. https://doi.org/10.3390/pharmaceutics13081288.

[22] D. Gupta, A.K. Singh, N. Kar, A. Dravid, J. Bellare, Modelling and optimization of NaOH-etched 3-D printed PCL for enhanced cellular attachment and growth with minimal loss of mechanical strength, Materials Science and Engineering: C 98 (2019) 602–611. https://doi.org/10.1016/j.msec.2018.12.084.

[23] A.L. Mutch, M.N. Gómez-Cerezo, L. Grøndahl, Surface functionalization of polycaprolactone-based biomaterials: Good practice and pitfalls, Biointerphases 20 (2025) 48501. https://doi.org/10.1116/6.0004773/3360494.

[24] T. Mohan, F. Gürer, D. Bračič, F. Lackner, C. Nagaraj, U. Maver, L. Gradišnik, M. Finšgar, R. Kargl, K.S. Kleinschek, Functionalization of Polycaprolactone 3D Scaffolds with Hyaluronic Acid Glycine-Peptide Conjugates and Endothelial Cell Adhesion, Biomacromolecules 26 (2025) 1771–1787. https://doi.org/10.1021/ACS.BIOMAC.4C01559.

[25] G. Salsano, C. Sardo, A. Guidone, P. Coppola, M. Sala, M.C. Scala, A. Soriente, M.G. Raucci, R.P. Aquino, G. Auriemma, Decoupling Bioactivity and Processability: RGD Click-Functionalized Coatings for a 3D-Printed PCL Scaffold, Biomacromolecules 26 (2025) 8234–8245. https://doi.org/10.1021/ACS.BIOMAC.5C01691.

[26] R.J. Hickey, A.E. Pelling, Cellulose biomaterials for tissue engineering, Front. Bioeng. Biotechnol. 7 (2019) 45. https://doi.org/10.3389/fbioe.2019.00045.

[27] S. Jin, X. Xia, J. Huang, C. Yuan, Y. Zuo, Y. Li, J. Li, Recent advances in PLGA-based biomaterials for bone tissue regeneration, Acta Biomater. 127 (2021) 56–79. https://doi.org/10.1016/J.ACTBIO.2021.03.067.

[28] L. Chen, J. Liu, M. Guan, T. Zhou, X. Duan, Z. Xiang, Growth Factor and Its Polymer Scaffold-Based Delivery System for Cartilage Tissue Engineering, Int. J. Nanomedicine 15 (2020) 6097–6111. https://doi.org/10.2147/IJN.S249829.

[29] C.H.T. Yew, P. Azari, J.R. Choi, F. Muhamad, B. Pingguan-Murphy, Electrospun Polycaprolactone Nanofibers as a Reaction Membrane for Lateral Flow Assay, Polymers (Basel). 10 (2018) 1387. https://doi.org/10.3390/polym10121387.

[30] C. Mircioiu, V. Voicu, V. Anuta, A. Tudose, C. Celia, D. Paolino, M. Fresta, R. Sandulovici, I. Mircioiu, Mathematical Modeling of Release Kinetics from Supramolecular Drug Delivery Systems, Pharmaceutics 11 (2019) 140. https://doi.org/10.3390/pharmaceutics11030140.

[31] A. Lisik, W. Musiał, Conductomeric Evaluation of the Release Kinetics of Active Substances from Pharmaceutical Preparations Containing Iron Ions, Materials 12 (2019) 730. https://doi.org/10.3390/ma12050730.

[32] Y. Nashchekina, A. Chabina, O. Moskalyuk, I. Voronkina, P. Evstigneeva, G. Vaganov, A. Nashchekin, V. Yudin, N. Mikhailova, Effect of Functionalization of the Polycaprolactone Film Surface on the Mechanical and Biological Properties of the Film Itself, Polymers (Basel). 14 (2022) 4654. https://doi.org/10.3390/polym14214654.

[33] J. Tan, Y. Liang, L. Sun, Z. Yang, J. Xu, D. Dong, H. Liu, Degradation Characteristics of Cellulose Acetate in Different Aqueous Conditions, Polymers (Basel). 15 (2023) 4505. https://doi.org/10.3390/polym15234505.

[34] D. Jyoti Mech, M. Suhail Rizvi, Micromechanics of fibrous scaffolds and their stiffness sensing by cells, Biomed. Mater. 19 (2024). https://doi.org/10.1088/1748-605X/ad2409.

[35] Y.D. Nokoorani, A. Shamloo, M. Bahadoran, H. Moravvej, Fabrication and characterization of scaffolds containing different amounts of allantoin for skin tissue engineering, Sci. Rep. 11 (2021) 16164. https://doi.org/10.1038/s41598-021-95763-4.

[36] A.R. Calore, V. Srinivas, S. Anand, A. Albillos-Sanchez, S.F.S.P. Looijmans, L.C.A. van Breemen, C. Mota, K. Bernaerts, J.A.W. Harings, L. Moroni, Shaping and properties of thermoplastic scaffolds in tissue regeneration: The effect of thermal history on polymer crystallization, surface characteristics and cell fate, J. Mater. Res. 36 (2021) 3914–3935. https://doi.org/10.1557/s43578-021-00403-2.

[37] B. Weng, F. Xu, M. Alcoutlabi, Y. Mao, K. Lozano, Fibrous cellulose membrane mass produced via forcespinning® for lithium-ion battery separators, Cellulose (London) 22 (2015) 1311–1320. https://doi.org/10.1007/s10570-015-0564-8.

[38] Z.-H. Hu, A.M. Omer, X. Ouyang, D. Yu, Fabrication of carboxylated cellulose nanocrystal/sodium alginate hydrogel beads for adsorption of Pb(II) from aqueous solution, Int. J. Biol. Macromol. 108 (2018) 149–157. https://doi.org/10.1016/j.ijbiomac.2017.11.171.

[39] J. Song, N.L. Birbach, J.P. Hinestroza, Deposition of silver nanoparticles on cellulosic fibers via stabilization of carboxymethyl groups, Cellulose 19 (2012) 411–424. https://doi.org/10.1007/s10570-011-9647-3.

[40] E. Zahedi, A. Esmaeili, N. Eslahi, M.A. Shokrgozar, A. Simchi, Fabrication and Characterization of Core-Shell Electrospun Fibrous Mats Containing Medicinal Herbs for Wound Healing and Skin Tissue Engineering, Mar. Drugs 17 (2019) 27. https://doi.org/10.3390/md17010027.

[41] R. Nithya, N. Meenakshi Sundaram, Biodegradation and cytotoxicity of ciprofloxacin-loaded hydroxyapatite-polycaprolactone nanocomposite film for sustainable bone implants, Int. J. Nanomedicine 10 Suppl 1 (2015) 119–127. https://doi.org/10.2147/IJN.S79995.

[42] S. Kim, M.C. Marcano, U. Becker, Effects of Hydroxyl and Carboxyl Functional Groups on Calcite Surface Wettability Using Atomic Force Microscopy and Density Functional Theory, ACS Earth Space Chem. 5 (2021) 2545–2554. https://doi.org/10.1021/acsearthspacechem.1c00240.

[43] F. Ghorbani, M. Sahranavard, Z. Mousavi Nejad, D. Li, A. Zamanian, B. Yu, Surface Functionalization of Three Dimensional-Printed Polycaprolactone-Bioactive Glass Scaffolds by Grafting GelMA Under UV Irradiation, Front. Mater. 7 (2020) 528590. https://doi.org/10.3389/FMATS.2020.528590/XML.

[44] E.M. Abdelrazek, A.M. Hezma, A. El-khodary, A.M. Elzayat, Spectroscopic studies and thermal properties of PCL/PMMA biopolymer blend, Egyptian Journal of Basic and Applied Sciences 3 (2016) 10–15. https://doi.org/10.1016/j.ejbas.2015.06.001.

[45] H. Palacios Hinestroza, H. Urena-Saborio, F. Zurita, A.A. Guerrero de León, G. Sundaram, B. Sulbarán-Rangel, Nanocellulose and Polycaprolactone Nanospun Composite Membranes and Their Potential for the Removal of Pollutants from Water, Molecules 25 (2020) 683. https://doi.org/10.3390/molecules25030683.

[46] N. Tuancharoensri, G.M. Ross, S. Mahasaranon, P.D. Topham, S. Ross, Ternary blend nanofibres of poly(lactic acid), polycaprolactone and cellulose acetate butyrate for skin tissue scaffolds: influence of blend ratio and polycaprolactone molecular mass on miscibility, morphology, crystallinity and thermal properties, Polym. Int. 66 (2017) 1463–1472. https://doi.org/10.1002/pi.5393.

[47] S. Park, J.O. Baker, M.E. Himmel, P.A. Parilla, D.K. Johnson, Cellulose crystallinity index: measurement techniques and their impact on interpreting cellulase performance, Biotechnol. Biofuels 3 (2010) 3. https://doi.org/10.1186/1754-6834-3-10.

[48] P. Morouço, S. Biscaia, T. Viana, M. Franco, C. Malça, A. Mateus, C. Moura, F.C. Ferreira, G. Mitchell, N.M. Alves, Fabrication of Poly(ε -caprolactone) Scaffolds Reinforced with Cellulose Nanofibers, with and without the Addition of Hydroxyapatite Nanoparticles, Biomed Res. Int. 2016 (2016) 1596110–1596157. https://doi.org/10.1155/2016/1596157.

[49] L. Kuang, J. Xiang, Z. He, The Functions and Mechanisms of TGF-β3 Signalling in Controlling the Fate Determinations of Various Types of Stem Cells, J. Cell. Physiol. 241 (2026) e70152. https://doi.org/10.1002/JCP.70152.

[50] L. Berten-Schunk, Y. Roger, H. Bunjes, A. Hoffmann, Release of TGF-β3 from Surface-Modified PCL Fiber Mats Triggers a Dose-Dependent Chondrogenic Differentiation of Human Mesenchymal Stromal Cells, Pharmaceutics 15 (2023). https://doi.org/10.3390/PHARMACEUTICS15041303.

[51] J. Sundermann, S. Sydow, L. Burmeister, A. Hoffmann, H. Menzel, H. Bunjes, Spatially and Temporally Controllable BMP-2 and TGF-β3 Double Release From Polycaprolactone Fiber Scaffolds via Chitosan-Based Polyelectrolyte Coatings, ACS Biomater. Sci. Eng. 10 (2024) 89–98. https://doi.org/10.1021/acsbiomaterials.1c01585.

[52] D. Barati, C. Gegg, F. Yang, Nanoparticle-Mediated TGF-β Release from Microribbon-Based Hydrogels Accelerates Stem Cell-Based Cartilage Formation In Vivo, Ann. Biomed. Eng. 48 (2020) 1971–1981. https://doi.org/10.1007/s10439-020-02522-z.

[53] H. V. Almeida, Y. Liu, G.M. Cunniffe, K.J. Mulhall, A. Matsiko, C.T. Buckley, F.J. O'Brien, D.J. Kelly, Controlled release of transforming growth factor-β3 from cartilage-extra-cellular-matrix-derived scaffolds to promote chondrogenesis of human-joint-tissue-derived stem cells, Acta Biomater. 10 (2014) 4400–4409. https://doi.org/10.1016/j.actbio.2014.05.030.

Declaration of interests

☐ The authors declare that they have no known competing financial interests or personal relationships that could have appeared to influence the work reported in this paper.

☒ The authors declare the following financial interests/personal relationships which may be considered as potential competing interests:

Edvinas Krugly reports financial support was provided by Research Council of Lithuania. If there are other authors, they declare that they have no known competing financial interests or personal relationships that could have appeared to influence the work reported in this paper.

Graphical abstract:

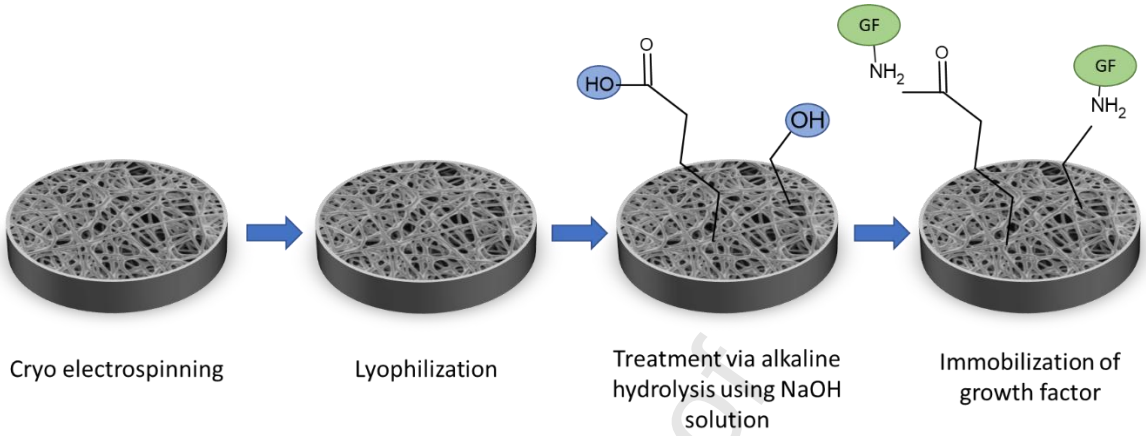

Highlights:

- Cryo-coaxial electrospinning produced porous PCL-HAP/CA core-shell scaffolds.
- Alkaline hydrolysis increased -COOH/-OH groups and deacetylated CA to cellulose.
- Water contact angle decreased by 82.6%, indicating improved wettability.
- Hydrolysis tuned fibre diameter and pore size, preserving core-shell architecture.
- Initial TGF-β3 burst release was reduced by 9%, enabling more sustained release.